

Boson-Peak-Like Anomaly Induced by Dipole Disordered States in $(\text{CH}_3\text{NH}_3)_4\text{InCl}_7$ Zhaolong Liu^{1,2}, Rui Luo,³ Munan Hao,^{1,2} Congcong Chai^{1,2},
Jiali Lu,^{1,2} Yurui Gao^{3,‡}, Shifeng Jin,^{1,†} and Xiaolong Chen^{1,4,5,*}¹Beijing National Laboratory for Condensed Matter Physics, Institute of Physics, Chinese Academy of Sciences, Beijing 100190, China²College of Materials Science and Opto-Electronic Technology, University of Chinese Academy of Sciences, Beijing 101408, China³Laboratory of Theoretical and Computational Nanoscience, National Center for Nanoscience and Technology, Chinese Academy of Sciences, Beijing 100190, China⁴School of Physical Sciences, University of Chinese Academy of Sciences, Beijing 100049, China⁵Songshan Lake Materials Laboratory, Dongguan 523808, China

(Received 10 April 2024; revised 10 July 2024; accepted 15 October 2024; published 20 November 2024)

Boson peaks are observed in glassy materials due to atom, spin, and strain disordered states that provide additional vibration modes at low temperatures. However, Boson peaks have not been observed in pure dipole disordered systems without structural disorder. Here, we report the observation of a Boson-peak-like hump in specific heat near 7 K in organic-inorganic hybrid crystal $MA_4\text{InCl}_7$ ($MA = \text{CH}_3\text{NH}_3$). The energy barrier for unbonded Cl anions migration is extremely low, allowing that the migration persists down to low temperatures. The migration and the subsequent relaxation process induce a random change in its dipole, leading to the dipole disorder states. Our results show that $MA_4\text{InCl}_7$ can be regarded as a dipole glass that can give rise to the Boson peak as well.

DOI: [10.1103/PhysRevLett.133.216101](https://doi.org/10.1103/PhysRevLett.133.216101)

Introduction—The harmonic vibrations of atoms in crystals are described by lattice waves and the quasi-particles (phonons) with quantified energies. The vibrational density of states (VDOS) can be well approximated by Debye’s model, that is, $g(\omega)$ proportional to ω^2 at low frequencies based on the assumption of uniform elastic medium at the long wavelength limit [1,2]. In 1971, Zeller and Pohl reported an abnormal hump in the low-temperature specific heat of glassy matters [3]. From the perspective of lattice, harmonic approximation cannot apply to amorphous materials. The additional phonon excitations caused by disordered structure result in higher VDOS than ones by the Debye approximation, which is manifested as the appearance of the Boson peaks near 5–10 K in the C_p/T^3 versus T diagram [4–8]. This deviation from the classical Debye model in the low temperature regime has been observed in almost all glassy materials, and is therefore considered to be a characteristic fingerprint of them [4,9,10].

Beyond structural glass and structural disordered crystals, such as the orientational glass, the term “ferroic glass” can be extended to encompass the disorder of additional physical quantities in crystalline materials, including magnetic moment, strain, and dipole [11]. Therefore, ferroic materials can exhibit three distinct ferroic glassy states: spin glass,

strain glass, and dipole glass (DPG) [11–16]. Analogous to conventional glassy materials, the disorder in these quantities may give rise to the Boson peak anomaly. In recent years, Boson peaks have been identified in spin glass [17,18], strain glass [19,20], and DPG systems exhibiting varying degrees of structural disorder [10,12]. However, it has been shown that even subtle structural disorder can trigger the appearance of Boson peaks and induce two-level systems (TLS) behavior [21]. To date, the pure dipole glass has not been isolated in a structurally ordered crystal to ascertain its specific contribution to the Boson peaks.

For a conventional ferroelectric, the dipoles are completely ordered (or absent) below (or above) its Curie temperature. It is difficult to attain a disordered dipole state [22,23]. Introducing foreign atoms through doping or creating vacancies in a ferroelectric material can lead to local disorder in the dipoles, while also causing structural disorder in the lattice. [12,14,24,25]. On the other hand, relaxor ferroelectrics may serve as potential candidates for a DPG during a certain duration after the electric field is switched off. But these transient disorder states are duration dependent and often mixed with other disordered forms, complicating precise characterizations at low temperatures [14–16]. In fact, in a polar structure, intrinsic dipoles generally experience minimal alterations, especially within the low temperature regime. If the energy barriers are low enough to allow one or two component ions consisting of a dipole to randomly migrate and change the amplitude or direction at relatively low frequencies, the dipole disorder state may be achieved. Unlike high-frequency ion

*Contact author: chenx29@iphy.ac.cn

†Contact author: shifengjin@iphy.ac.cn

‡Contact author: gaoyr@nanoctr.cn

vibrations, the low frequency migrations enable the excitation of dipoles as additional modes at low temperatures [11,26,27]. Recently, substantial enhancements of polarization have been observed due to ion migrations in organic-inorganic hybrid crystals in low frequencies [28,29], motivating us to explore DPG states in similar compounds.

In this Letter, we report the observation of an abnormal hump in specific heat at around 7 K, similar to the Boson peak of glassy matters in the structurally ordered MA_4InCl_7 single crystal. It exhibits giant polarizations ($\sim 20\,860\ \mu\text{C cm}^{-2}$) under low frequency electric fields ($\sim 12.5\ \text{mHz}$) caused by Cl anions migrations. Density functional theory (DFT) calculations reveal that Cl anions migrations in thermodynamic vibration level ($\sim 0.1\ \text{\AA}$) are allowed at temperatures as low as 7 K and induce the random change in dipoles. We propose that MA_4InCl_7 is a dipole glass and the specific heat anomaly may due to the dipole disorder states.

Crystal structure analysis—The crystal structure of MA_4InCl_7 was previously reported to be centrosymmetric in space group $P2/n$ (No. 13) [30–32]. Here, we have redetermined the space group as non-centrosymmetric Pn (No. 7) using single crystals grown by evaporative crystallization [Fig. 1(a)]. This reassignment was supported by

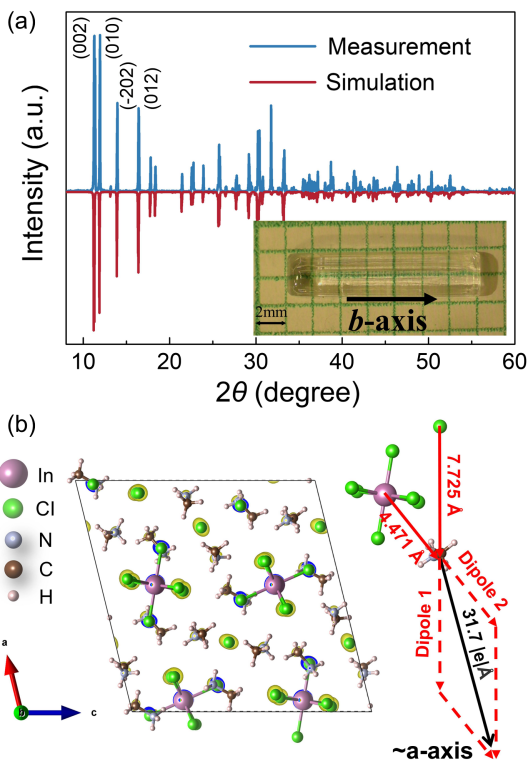


FIG. 1. (a) Experimental and simulated powder x-ray diffraction (PXRD) patterns of MA_4InCl_7 at room temperature. The insert shows the photo of MA_4InCl_7 single crystal. (b) On the left is the single crystal structure of MA_4InCl_7 , and on the right is the schematic diagram of dipole moment synthesis along the a axis, where $31.7|e|\ \text{\AA}$ represents the a axis dipole moment of the whole unit cell. The yellow ellipsoid represents the charge density.

second harmonic generations (SHG) measurement, where a clear signal was observed in MA_4InCl_7 [Fig. S1]. The single crystal x-ray diffraction (SCXRD) data are presented in Table S1 and Table S2 in the Supplemental Material [33]. As shown in Fig. 1(b), indium cations are coordinated with six Cl anions to form two types of distorted octahedra. Additionally, unbonded Cl anions reside between the two $[InCl_6]^{3-}$ octahedrons. The noncentrosymmetric Pn (No. 7) allows the presence of dipoles in the ac plane. In this case, the calculated dipole is approximately $31.7|e|\ \text{\AA}$ in magnitude and almost along the a axis in the direction starting from the Cl anions and the octahedrons toward the positively charged $[CH_3NH_3]^+$ [Fig. 1(b)].

Polarization measurements—The variations of polarization versus electric field (P - E) and current density versus electric field (J - E) were measured on a MA_4InCl_7 single crystal along the b axis under an ac electric field of 12.5 mHz [Fig. 2(a)]. The P - E curve resembles the hysteresis loop of ferroelectrics but exhibits a remarkable remnant polarization up to $20\,860\ \mu\text{C cm}^{-2}$. Notably, for space group Pn , the hysteresis loop along the b axis should not exist [48,49]. A striking feature is that the polarization of MA_4InCl_7 only emerges under a low frequency ac electric field. As depicted in Fig. 2(b), the saturated polarization decreases with the increasing frequency of the electric field and is not detectable at 50 Hz [Fig. S2 [33]]. This behavior suggests that ion migration under an electric field leads to polarization, differing from conventional ferroelectrics [28]. Under an electric field, ions become more mobile, ultimately resulting in long-range migrations and macroscopic polarization. When the frequency is too high, ion migrations cannot keep pace, resulting in no change in polarization. Additionally, polarization relaxation is observed upon switching off the field. Its value gradually decreases with delay time and can be fitted by an exponential curve [Fig. 2(c)]. This yields a characteristic relaxation time of approximately $\sim 5.6\ \text{min}$, representing the duration needed for mobile ions to return to their original positions. This observation is supported by the current variations induced by re-polarization with delay-time shown in Fig. 2(e). The current peaks can reach a maximum at about $10\ \mu\text{A}$ only when the delay time exceeds 7 min, in agreement with the characteristic relaxation time.

To identify the ions responsible for the observed polarization, we coated a thin layer of silver paste on the crystal surface. Energy dispersive spectrometer (EDS) measurements showed a 1:1 ratio of Ag to Cl on the top electrode after multiple polarizations, suggesting the formation of AgCl. In contrast, no Cl element was observed on the opposite electrode [Fig. S3 [33]]. The mobility of Cl anions under an electric field aligns with the structural characteristics of MA_4InCl_7 described above.

If we assume that the polarization of approximately $\sim 20\,860\ \mu\text{C cm}^{-2}$ under a field of $5\ \text{kV cm}^{-1}$ is primarily

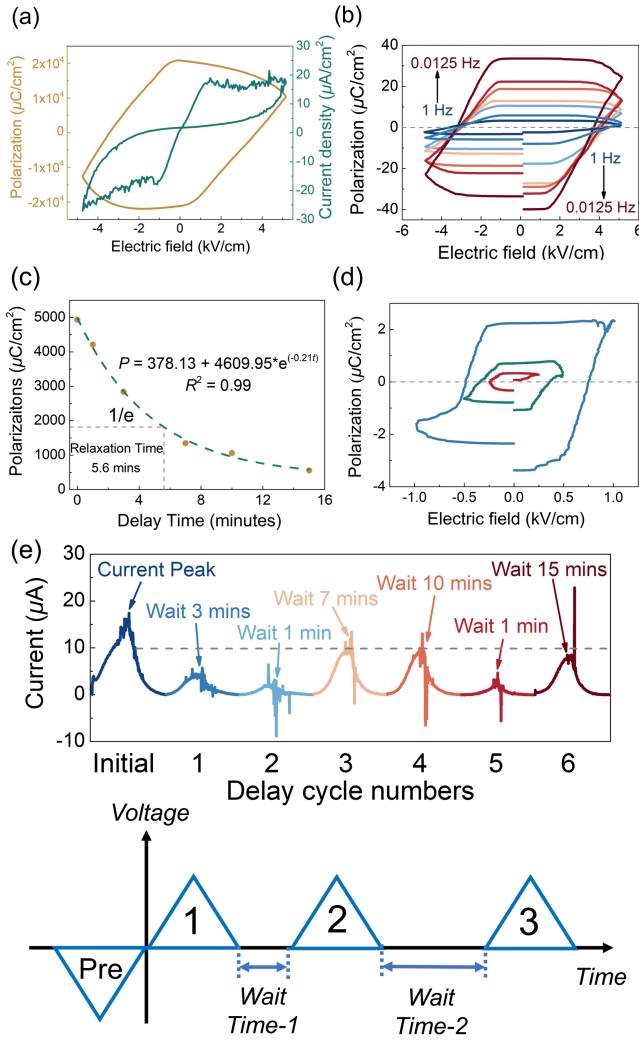


FIG. 2. (a) The P - E and J - E curves of MA_4InCl_7 . (b) Frequency dependence of P - E curves, tested from 12.5 mHz to 1 Hz. (c) Delay-time variation of the polarization. The green dashed line represents an exponential fitting curve, with a relaxation time of ~ 5.6 min. (d) The P - E curves under low electric fields, tested from 0.25 to 1 $kV\ cm^{-1}$. (e) The pulse program and delay-time variation of the current peak values of MA_4InCl_7 , with the first test current peak undergoing reverse pre-polarization. The test frequency was 12.5 mHz in the (a) and (d) panels.

due to the migration of unbonded Cl anions, the calculated average migration distance for each Cl anions is 0.62 μm , equivalent to approximately 831 lattice cells (refer to Supplemental Material [33] for more details). Notably, even at a low electric field of 0.25 $kV\ cm^{-1}$, MA_4InCl_7 can display a hysteresis loop with a polarization of 0.32 $\mu C\ cm^{-2}$ [Fig. 2(d)]. The calculated migration distance of unbonded Cl anions is 0.096 \AA , only around 0.05 times the radius of the Cl anion. This short-range migration distance falls well within the thermal displacement of their equilibrium positions $(\overline{u^2})^{1/2} \sim 0.26\ \text{\AA}$ (Table S3 [33]). This suggests that the vibrations of unbonded Cl anions always induce the polarization and subsequent relaxation in

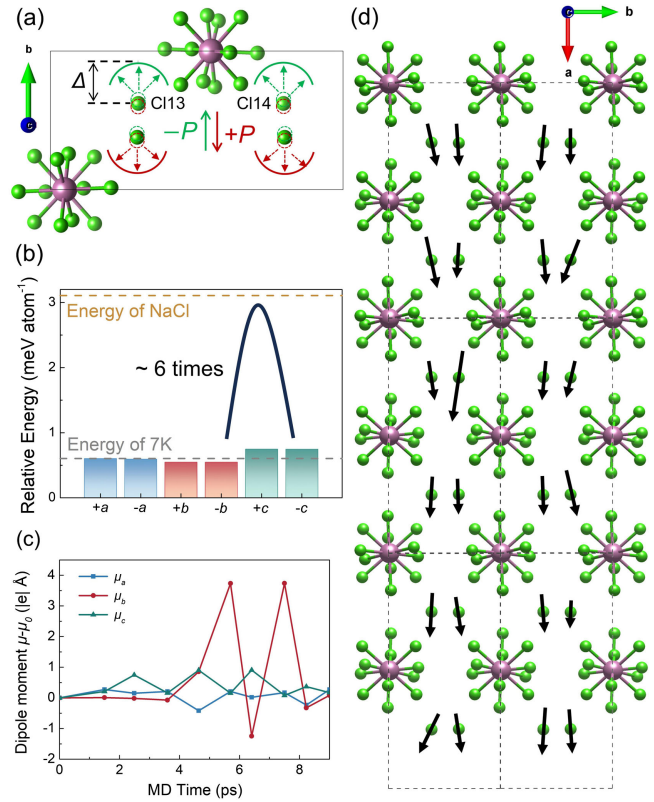


FIG. 3. (a) Schematic dipoles introduced by shifts in unbonded Cl anions, where Δ represents the shift amplitude ($\sim 0.1\ \text{\AA}$). (b) The relative energy required for unbonded Cl anions in MA_4InCl_7 to shift by 0.1 \AA along different directions. The gray dashed line represents the energy corresponding to 7 K and the yellow dashed line represents the energy required for Cl anions in NaCl to shift by 0.1 \AA . (c) The dipole moment versus time in AIMD simulation of MA_4InCl_7 at 7 K after subtracting initial μ_0 . (d) Diagram of the dipole glass state caused by ion shifts, where the black arrows represent the dipole contributed by unbonded Cl anions. For simplicity, the methylamine group are omitted in the (a) and (d) panels.

low frequencies. Consequently, even in the absence of an electric field, Cl anions can still undergo the low-frequency vibrations.

We then performed DFT calculations to assess the dipole moments and energy barriers when the four unbonded Cl anions in the MA_4InCl_7 cell vibrate in the a , b , and c directions, respectively [Fig. 3(a)]. For instance, considering a shift of 0.1 \AA from their equilibrium positions for the Cl anions, the results are listed in Table I. Initially, the structure exhibits no dipole component along the b direction, but values of 31.70 and 0.28 $|e|$ \AA are observed along the a direction and c direction, respectively, indicating the dipoles primarily align along the a axis. The dipole component along the b axis (μ_b) will remain at zero unless the shift occurs in the same direction. If the Cl anions shift by 0.1 \AA along the b axis, μ_b reaches $\sim 0.503|e|$ \AA , corresponding to a polarization of $\sim 0.42\ \mu C\ cm^{-2}$, which closely matches the experimental value of 0.32 $\mu C\ cm^{-2}$.

TABLE I. Dipole components (μ_a, μ_b, μ_c) and barrier energy of MA_4InCl_7 for unbonded Cl anions shift 0.1 Å along the a , b , and c directions. $1|e| \text{ Å}$ equals to $0.8416 \mu\text{C cm}^{-2}$ in MA_4InCl_7 .

	$\mu_a(e \text{Å})$	$\mu_b(e \text{Å})$	$\mu_c(e \text{Å})$	Relative energy (meV atom $^{-1}$)
Initial	-31.6953	-0.0000	-0.2788	0
a direction	-32.7550	0.0032	-0.1172	0.6027
$-a$ direction	-31.8644	-0.0030	0.0753	0.5939
b direction	-32.2994	-0.5030	-0.0169	0.5466
$-b$ direction	-32.3204	0.5032	-0.0253	0.5470
c direction	-32.3898	0.0012	-0.5601	0.7467
$-c$ direction	-32.2302	-0.0011	0.5178	0.7458

The energy barriers for the short-range migrations of unbonded Cl anions are dependent on crystallographic direction, with the lowest barrier of $\sim 0.547 \text{ meV atom}^{-1}$ along the b axis [Fig. 3(b)]. So, it is anticipated that the shift amplitude will differ along the three directions at the same temperature, resulting in a random change in the dipole vector. Additionally, the *ab initio* molecular dynamic (AIMD) simulation was performed for MA_4InCl_7 at 7 K. The snapshots of the structure at different time, as shown in Fig. S4 [33], reveal the shifts of Cl anions while the methylamine groups remain relatively unchanged. Subsequently, the corresponding dipole moments of MA_4InCl_7 were calculated. Upon subtracting the initial dipole μ_0 , it is observed that the dipole vector varies over time [Fig. 3(c)]. Statistically, this indicates a dipole disordered state [Fig. 3(d)]. Moreover, this state can persist at low temperatures $\sim 7 \text{ K}$, as the ions can still shift and tend to migrate along the b axis, given that kT is larger than 0.547 meV .

Specific heat measurement—We performed low-temperature specific heat measurement on MA_4InCl_7 single crystals. Because of its large direct band gap of 4.18 eV, the contribution of electrons to the specific heat at low temperatures can be neglected (Fig. S5 in Supplemental Material [33]). Notably, no phase transition peak appears below 40 K [Fig. 4(a)]. To quantitatively assess the contribution of the two-level systems (TLS), we conducted quadratic fits of C_p/T against T^2 for MA_4InCl_7 , NaCl, ferroelectric crystal TGS, and $[(\text{CH}_3)_4\text{N}]_4\text{In}_2\text{Cl}_9 \cdot 3\text{H}_2\text{O}$ (CNICH, an orientational disordered compound with structure shown in Fig. S6 [33]) [Fig. 4(b)]. We employed the formula $C_p = \gamma T + \beta T^3 + wT^5$ for fitting, where γ , β , and w represent the coefficients of the contributions from TLS, Debye acoustic modes, and additional modes, respectively [10,50–52]. The obtained coefficients are displayed in Table S4 [33]. By plotting C_p/T^3 versus T curve on a logarithmic scale, we observe that a Boson-peak-like hump appears in MA_4InCl_7 near 7 K [Fig. 4(c)]. The data presented in Fig. 4(d) highlight the departure from harmonic Debye behavior, evident as an upturn at low temperatures. Unlike ordered crystals, the Boson peaks and upturns of various glasses exhibit a similar shape

regardless of their nature. In comparison, a strong Boson peak appears at 5 K in CNICH (Fig. S7 [33]). The peaks for TGS and NaCl single crystals appear around 15–25 K and then tend to Debye-like levels at lower temperatures, a characteristic behavior of crystalline matters [Fig. 4(c)]. The contribution of long-range ordered dipoles to the specific heat in TGS appears to be minimal, if present at all. In contrast, the chaotic dipole states in MA_4InCl_7 make a significant contribution to the specific heat, similar to that observed in CNICH. Meanwhile, after being polarized by varying electric fields, the measured specific heat data of MA_4InCl_7 are similar to that without pre-polarization, indicating that chaotic dipole states are intrinsic, not induced by the electric field.

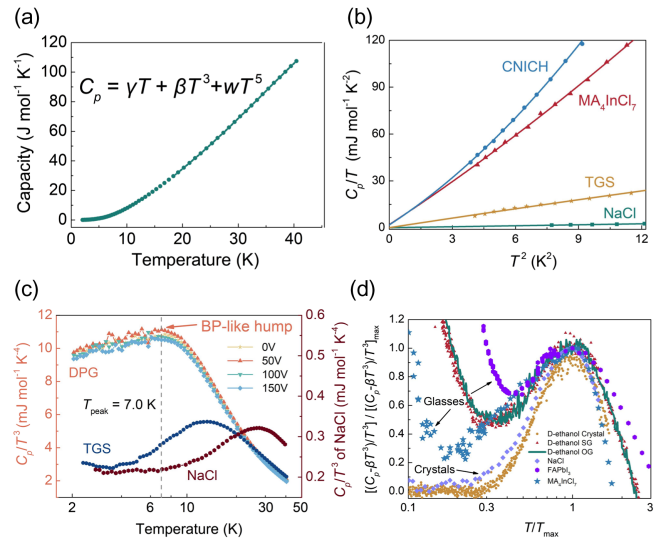


FIG. 4. (a) The specific heat of MA_4InCl_7 in the temperature range of 2–40 K. (b) Diagram of C_p/T versus T^2 relation of CNICH, MA_4InCl_7 (DPG), TGS, and NaCl crystal. It also uses a quadratic fit to obtain the linear, cubic, and fifth-power coefficients of heat capacity. (c) C_p/T^3 versus T relation of MA_4InCl_7 , ferroelectric TGS and single crystal NaCl. (d) Normalized specific-heat data based on β values. D ethanol has three counterparts, which are crystal, structural glass (SG) and orientational glass (OG) [53]. This figure has been modified according to Ref. [52].

The presence of the hump can be ascribed to additional excitable modes at low temperature for $MA_4\text{InCl}_7$ due to disordered dipoles. TGS, on the other hand, is more similar to NaCl in low temperature specific heat, indicating a lack of excitable modes caused by disordered dipoles. Table S5 lists the dipole and atom ordered and disordered states [33]. The key factor to the observation of Boson-peak-like hump is the presence of the dipole disordered states induced by Cl anions migration and relaxation processes, which can persist down to low temperatures. Strong and distinct Boson peaks have been observed in lead-iodine-based hybrid perovskites such as FAPbI_3 (FA = Formamidinium) [54,55]. In contrast to $MA_4\text{InCl}_7$, the “glassy anomalies” in these hybrid perovskites may primarily stem from the high orientational disorder of organic cations in their structures. Studies [21] have shown that even subtle structural disorder can lead to the emergence of Boson peaks and TLS behavior. The observation of glass anomaly behavior in the structurally fully ordered $MA_4\text{InCl}_7$ single crystals eliminate the contribution of structural disorders on the heat capacity, thereby isolating the contribution of dipole disorders only.

The emergence of vibrational dipole states is associated with high anisotropy, low potential barriers, and low frequency relaxations. We calculated the vibrational barrier energy of NaCl crystals to be $3.108 \text{ meV atom}^{-1}$, approximately 6 times that of $MA_4\text{InCl}_7$ (Table S6 in the Supplemental Material [33]). The strong ionic bonds in NaCl lead to large potential barriers for atomic vibrations, hardly inducing excitable dipole states at low temperatures. However, in $MA_4\text{InCl}_7$, the unbonded Cl anions are distant from the $[\text{InCl}_6]^{3-}$ groups and only form weak hydrogen bonds with the methylamine. The vibrations or migration encounter a smaller steric resistance. Furthermore, the relaxation behavior implies that Cl anions require a certain time to return to their initial state, unlike the harmonic vibrational behavior in conventional crystals. It hinders ion migrations, similar to the “phonon damping” in amorphous materials [56–59]. Consequently, it serves as the condition for the formation of dipole disordered states and the source of Boson peak anomalies.

Conclusions—We propose that $MA_4\text{InCl}_7$ can be regarded as a dipole glass without structural disorder based on structural analyses, polarization measurements and DFT calculations. An abnormal hump in the specific heat data was observed near 7 K in the $MA_4\text{InCl}_7$ single crystal, which can be attributed to the existence of dipole disordered states, resembling the observations in spin glass and strain glass. Furthermore, the observations of the TLS linear term and upturn at ultralow temperature of $MA_4\text{InCl}_7$ evidence that the tunneling model is also effective in dipole glass. This work offers new insights into the origin of Boson peaks, and introduces a new concept of dipole glass as a source of Boson peak anomalies in the absence of structural disorder.

Acknowledgments—We thank Shiliang Li for his assistance in the ultralow temperature specific heat measurements. This work is financially supported by the Strategic Priority Research Program and Key Research Program of Frontier Sciences of the Chinese Academy of Sciences (Grant No. XDB33010100), National Natural Science Foundation of China (Grants No. 52272268 and No. 22273014), and the National Key Research and Development Program (Grant No. 2022YFA1203200). This work was supported by the Synergetic Extreme Condition User Facility (SECUF).

-
- [1] C. Kittel, *Introduction to Solid State Physics* (Wiley, New York, 2004).
 - [2] J. Yang, Y. J. Wang, E. Ma, A. Zaccone, L. H. Dai, and M. Q. Jiang, Structural parameter of orientational order to predict the Boson vibrational anomaly in glasses, *Phys. Rev. Lett.* **122**, 015501 (2019).
 - [3] R. C. Zeller and R. O. Pohl, Thermal conductivity and specific heat of noncrystalline solids, *Phys. Rev. B* **4**, 2029 (1971).
 - [4] W. A. Phillips, *Amorphous Solids: Low Temperature Properties* (Springer, Berlin, 1981).
 - [5] A. N. Vasiliev, T. N. Voloshok, A. V. Granato, D. M. Joncich, Y. P. Mitrofanov, and V. A. Khonik, Relationship between low-temperature boson heat capacity peak and high-temperature shear modulus relaxation in a metallic glass, *Phys. Rev. B* **80**, 172102 (2009).
 - [6] S. Gelin, H. Tanaka, and A. Lemaître, Anomalous phonon scattering and elastic correlations in amorphous solids, *Nat. Mater.* **15**, 1177 (2016).
 - [7] Y. C. Hu and H. Tanaka, Origin of the boson peak in amorphous solids, *Nat. Phys.* **18**, 669 (2022).
 - [8] M. Tømterud, S. D. Eder, C. Büchner, L. Wondraczek, I. Simonsen, W. Schirmacher, J. R. Manson, and B. Holst, Observation of the boson peak in a two-dimensional material, *Nat. Phys.* **19**, 1910 (2023).
 - [9] Y. G. Vainer, A. V. Naumov, M. Bauer, and L. Kador, Experimental evidence of the local character of vibrations constituting the Boson peak in amorphous solids, *Phys. Rev. Lett.* **97**, 185501 (2006).
 - [10] M. A. Ramos, *Low-Temperature Thermal and Vibrational Properties of Disordered Solids* (World Scientific, Singapore, 2022).
 - [11] G. Burns and F. H. Dacol, Crystalline ferroelectrics with glassy polarization behavior, *Phys. Rev. B* **28**, 2527 (1983).
 - [12] X. B. Ren, Strain glass and ferroic glass—Unusual properties from glassy nano-domains, *Phys. Status Solidi (b)* **251**, 1982 (2014).
 - [13] J. A. Mydosh, *Spin-Glasses: An Experimental Introduction* (Taylor and Francis, London, 1993).
 - [14] L. E. Cross, Relaxor ferroelectrics, *Ferroelectrics* **76**, 241 (1987).
 - [15] D. Viehland, S. J. Jang, L. E. Cross, and M. Wuttig, Deviation from Curie-Weiss behavior in relaxor ferroelectrics, *Phys. Rev. B* **46**, 8003 (1992).

- [16] G. Shabbir and S. Kojima, Low-temperature elastic properties of lanthanum lead zirconate titanate relaxor ferroelectric ceramics, *J. Korean Phys. Soc.* **46**, 128 (2005).
- [17] M. Kofu, R. Watanuki, T. Sakakibara, S. Ohira-Kawamura, K. Nakajima, M. Matsuura, T. Ueki, K. Akutsu, and O. Yamamuro, Spin glass behavior and magnetic boson peak in a structural glass of a magnetic ionic liquid, *Sci. Rep.* **11**, 12098 (2021).
- [18] M. Kofu, S. Ohira-Kawamura, N. Murai, R. Ishii, D. Hirai, H. Arima, and K. Funakoshi, Magnetic boson peak in classical spin glasses, *Phys. Rev. Res.* **6**, 013006 (2024).
- [19] S. Ren, H. X. Zong, X. F. Tao, Y. H. Sun, B. A. Sun, D. Z. Xue, X. D. Ding, and W. H. Wang, Boson-peak-like anomaly caused by transverse phonon softening in strain glass, *Nat. Commun.* **12**, 5755 (2021).
- [20] H. Lin *et al.*, Strain glass in $\text{Ti}_{50-x-y}\text{Ni}_{50+y}\text{Nb}_y$ alloys exhibiting a boson peak glassy anomaly, *Scr. Mater.* **224**, 115118 (2023).
- [21] J. F. Gebbia, M. A. Ramos, D. Szewczyk, A. Jezowski, A. I. Krivchikov, Y. V. Horbatenko, T. Guidi, F. J. Bermejo, and J. L. Tamarit, Glassy anomalies in the low-temperature thermal properties of a minimally disordered crystalline solid, *Phys. Rev. Lett.* **119**, 215506 (2017).
- [22] V. K. Wadhavan, *Introduction to Ferroic Materials* (CRC, Boca Raton, FL, 2000).
- [23] W. Zhang and R. G. Xiong, Ferroelectric metal-organic frameworks, *Chem. Rev.* **112**, 1163 (2012).
- [24] T. Y. Kim and H. M. Jang, B-site vacancy as the origin of spontaneous normal-to-relaxor ferroelectric transitions in La-modified PbTiO_3 , *Appl. Phys. Lett.* **77**, 3824 (2000).
- [25] R. Zhang, J. F. Li, and D. Viehland, Effect of aliovalent substituents on the ferroelectric properties of modified barium titanate ceramics—relaxor ferroelectric behavior, *J. Am. Ceram. Soc.* **87**, 864 (2004).
- [26] Y. Wang, S. Shang, Z. K. Liu, and L. Q. Chen, Mixed-space approach for calculation of vibration-induced dipole-dipole interactions, *Phys. Rev. B* **85**, 224303 (2012).
- [27] S. Hou and P. F. Bernath, Relationship between dipole moments and harmonic vibrational frequencies in diatomic molecules, *J. Phys. Chem. A* **119**, 1435 (2015).
- [28] J. Lu, R. Luo, J. Zhou, M. Hao, C. Chai, T. Ying, Y. Gao, S. Jin, and X. Chen, High, multiple, and nonvolatile polarizations in organic-inorganic hybrid $[(\text{CH}_3)_3(\text{CH}_2\text{CH}_2\text{Cl})\text{N}]_2\text{InCl}_5 \cdot \text{H}_2\text{O}$ for memcapacitor, *J. Am. Chem. Soc.* **146**, 281 (2024).
- [29] J. Yanagisawa *et al.*, Strongly enhanced polarization in a ferroelectric crystal by conduction-proton flow, *J. Am. Chem. Soc.* **146**, 1476 (2024).
- [30] H. U. Schlimper and M. L. Ziegler, The crystal structure of $(\text{CH}_3\text{NH}_3)_4\text{InCl}_7$, *Z. Naturforsch. B* **27**, 377 (1972).
- [31] F. Lin, G. Yu, S. Weng, C. Zhou, Y. Han, W. Liu, K. Zhou, Y. Wang, and H. Lin, Blue photoluminescence enhancement achieved by zero-dimensional organic indium halides via a metal ion doping strategy, *Mater. Chem. Front.* **7**, 137 (2023).
- [32] D. Liang, X. Liu, B. Luo, Q. Qian, W. Cai, S. Zhao, J. Chen, and Z. Zang, High quantum yield of In-based halide perovskites for white light emission and flexible x-ray scintillators, *EcoMat* **5**, e12296 (2023).
- [33] See Supplemental Material at <http://link.aps.org/supplemental/10.1103/PhysRevLett.133.216101> for more details of the experimental process and analytical calculations, which includes Refs. [34–47].
- [34] G. M. Sheldrick, SHELXT—Integrated space-group and crystal-structure determination, *Acta Crystallogr. Sect. A* **71**, 3 (2015).
- [35] G. M. Sheldrick, Crystal structure refinement with SHELXL, *Acta Crystallogr. Sect. C* **71**, 3 (2015).
- [36] O. V. Dolomanov, L. J. Bourhis, R. J. Gildea, J. A. K. Howard, and H. Puschmann, OLEX2: A complete structure solution, refinement and analysis program, *J. Appl. Crystallogr.* **42**, 339 (2009).
- [37] A. A. Belik, T. Ikeda, F. Izumi, and K. Momma, Dysnomia, a computer program for maximum-entropy method (MEM) analysis and its performance in the MEM-based pattern fitting, *Powder Diffr.* **28**, 184 (2013).
- [38] G. Kresse and J. Furthmüller, Efficient iterative schemes for *ab initio* total-energy calculations using a plane-wave basis set, *Phys. Rev. B* **54**, 11169 (1996).
- [39] P. E. Blöchl, Projector augmented-wave method, *Phys. Rev. B* **50**, 17953 (1994).
- [40] J. P. Perdew, K. Burke, and M. Ernzerhof, Generalized gradient approximation made simple, *Phys. Rev. Lett.* **77**, 3865 (1996).
- [41] G. Henkelman, B. P. Uberuaga, and H. Jónsson, A climbing image nudged elastic band method for finding saddle points and minimum energy paths, *J. Chem. Phys.* **113**, 9901 (2000).
- [42] D. Sheppard, R. Terrell, and G. Henkelman, Optimization methods for finding minimum energy paths, *J. Chem. Phys.* **128**, 134106 (2008).
- [43] H. J. Monkhorst and J. D. Pack, Special points for Brillouin-zone integrations, *Phys. Rev. B* **13**, 5188 (1976).
- [44] K. S. Cole and R. H. Cole, Dispersion and absorption in dielectrics I. Alternating current characteristics, *J. Chem. Phys.* **9**, 341 (1941).
- [45] J. J. De Yoreo, R. O. Pohl, and G. Burns, Low-temperature thermal properties of ferroelectrics, *Phys. Rev. B* **32**, 5780 (1985).
- [46] I. Henning, P. Frach, E. Hegenbarth, and V. I. Ffutsbefg, Glass-like behaviour of PLZT demonstrated by heat capacity measurements, *Phys. Status Solidi A* **70**, K7 (1982).
- [47] I. Henning, M. Mertig, R. Plath, G. Pompe, E. Hegenbarth, and R. Schalge, Glass-like behaviour of $\text{Sr}_{1-x}\text{Ba}_x\text{Nb}_2\text{O}_6$ (SBN) single crystals demonstrated by heat capacity measurements, *Phys. Status. Solidi. A* **73**, K105 (1982).
- [48] K. Aizu, Symmetries in the paraelectric phase-transformations of ferroelectric crystals, *J. Phys. Soc. Jpn.* **19**, 918 (1964).
- [49] P. P. Shi, Y. Y. Tang, P. F. Li, W. Q. Liao, Z. X. Wang, Q. Ye, and R. G. Xiong, Symmetry breaking in molecular ferroelectrics, *Chem. Soc. Rev.* **45**, 3811 (2016).
- [50] P. W. Anderson, B. I. Halperin, and C. M. Varma, Anomalous thermal properties of glasses and spin glasses, *Philos. Mag.* **25**, 1 (1972).
- [51] W. A. Phillips, Tunneling states in amorphous solids, *J. Low Temp. Phys.* **7**, 351 (1972).
- [52] M. Moratalla, J. F. Gebbia, M. A. Ramos, L. C. Pardo, S. Mukhopadhyay, S. Rudić, F. Fernandez-Alonso,

- F. J. Bermejo, and J. L. Tamarit, Emergence of glassy features in halomethane crystals, *Phys. Rev. B* **99**, 024301 (2019).
- [53] C. Talón, M. A. Ramos, and S. Vieira, Low-temperature specific heat of amorphous, orientational glass, and crystal phases of ethanol, *Phys. Rev. B* **66**, 012201 (2002).
- [54] S. Kawachi, M. Atsumi, N. Saito, N. Ohashi, Y. Murakami, and J.-i. Yamaura, Structural and thermal properties in formamidinium and Cs-mixed lead halides, *J. Phys. Chem. Lett.* **10**, 6967 (2019).
- [55] D. H. Fabini, T. Hogan, H. A. Evans, C. C. Stoumpos, M. G. Kanatzidis, and R. Seshadri, Dielectric and thermodynamic signatures of low-temperature glassy dynamics in the hybrid perovskites $\text{CH}_3\text{NH}_3\text{PbI}_3$ and $\text{HC}(\text{NH}_2)_2\text{PbI}_3$, *J. Phys. Chem. Lett.* **7**, 376 (2016).
- [56] V. Lubchenko and P. G. Wolynes, The origin of the boson peak and thermal conductivity plateau in low-temperature glasses, *Proc. Natl. Acad. Sci. U.S.A.* **100**, 1515 (2003).

- [57] L. E. Bove, C. Petrillo, A. Fontana, and A. P. Sokolov, Damping of sound waves in the terahertz range and strength of the boson peak, *J. Chem. Phys.* **128**, 184502 (2008).
- [58] M. Baggioli and A. Zaccone, Universal origin of Boson peak vibrational anomalies in ordered crystals and in amorphous materials, *Phys. Rev. Lett.* **122**, 145501 (2019).
- [59] Q. Guo, H. P. Zhang, Z. Lu, H. Y. Bai, P. Wen, and W. H. Wang, Boson peak: Damped phonon in solids, *Appl. Phys. Lett.* **121**, 142204 (2022).
- [60] A. Francisco-López, B. Charles, M. I. Alonso, M. Garriga, M. Campoy-Quiles, M. T. Weller, and A. R. Goñi, Phase diagram of methylammonium /formamidinium lead iodide perovskite solid solutions from temperature-dependent photoluminescence and Raman spectroscopies, *J. Phys. Chem. C* **124**, 3448 (2020).

End Matter

Appendix A: Raman scattering—As mentioned in the Letter, the phenomenon of “Boson peak” has also been reported in some lead-iodine-based hybrid perovskites, such as MAPbI_3 , FAPbI_3 and their solid solutions [54,55]. Unlike MA_4InCl_7 , which has fully ordered occupancy and orientation, both the MA and FA lead iodide systems exhibit a high degree of orientational disorder in organic groups. We have analyzed the Raman spectra for different materials. As shown in Fig. 5(a), ordered crystal structures possess highly consistent bond angles and bond lengths, which are arranged in an orderly manner and generally exhibit sharp Raman peaks, resulting in characteristic strong scattering bands. For instance, NaCl , Si , and MA_4InCl_7 exhibit such characteristics. However, amorphous structures or orientationally disordered

materials exhibit a wide range of bond angle and bond length fluctuations, resulting in broadened Raman peaks due to the possible distribution of states, such as FAPbI_3 , $\text{FA}_{0.3}\text{MA}_{0.7}\text{PbI}_3$ and conventional glass [60]. Therefore, the intense Boson peaks observed in FAPbI_3 and its solid solutions should mainly due to the orientational disorder behavior of the organic cations, and those materials have been classified into the category of orientational glass. Moreover, as shown in Fig. 5(b), MAPbI_3 exhibits dynamic orientational disorder at high temperatures, leading to broadened peaks in the Raman spectrum. Conversely, at low temperatures, the motion of MA^+ groups gradually freeze, leading to their locking within inorganic cages. This vanishing dynamical disorder is reflected in the marked reduction of the inhomogeneous

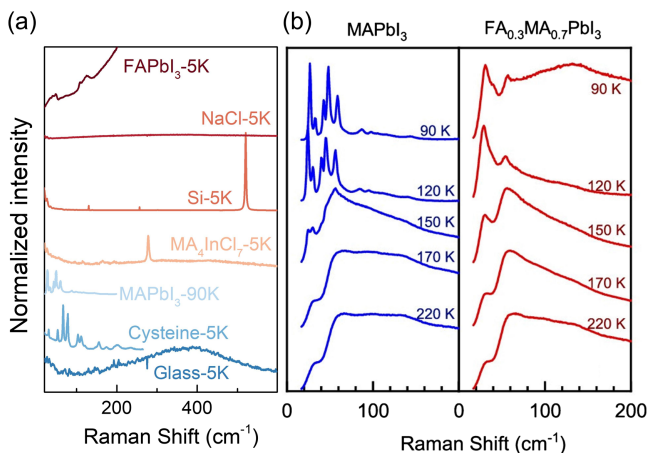


FIG. 5. (a) Raman spectra of materials with different structures at various temperatures. (b) Raman spectra of MAPbI_3 single crystal (left panel) and one with 30% FA content (right panel) at different temperatures [60]. The spectra were normalized and shifted vertically for clarity.

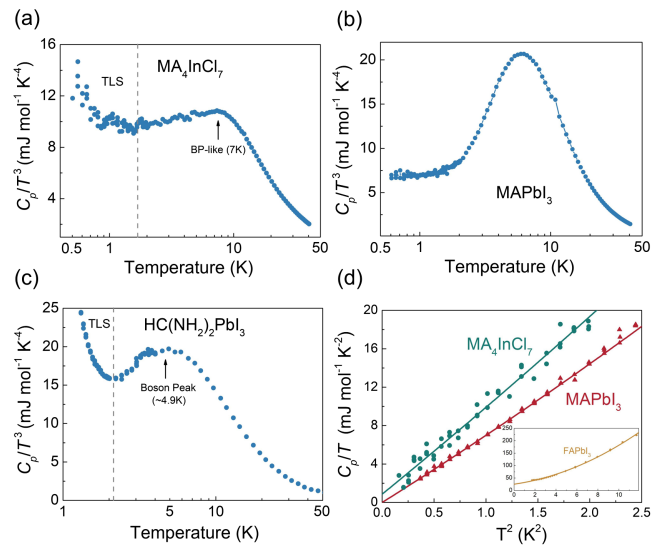


FIG. 6. C_p/T^3 versus T relation of MA_4InCl_7 (a), MAPbI_3 (b), and FAPbI_3 (c). (d) The C_p/T vs T^2 curves are fitted for MA_4InCl_7 , MAPbI_3 , and FAPbI_3 to a quadratic polynomial.

broadening of Raman peaks and the emergence of vibrational modes at lower wave numbers [60]. Further distinctions between the behavior of MA_4InCl_7 and $MAPbI_3$ at low temperatures are evident in the ultralow temperature specific heat data presented here.

Appendix B: Ultralow temperature specific heat—We collected heat capacity data at ultralow temperatures down to 0.5 K to assess the TLS contribution, a universal characteristic of glassy states. The linear term of TLS does exist in the insulating MA_4InCl_7 single crystal, as revealed by the low temperature heat capacity data shown in Figs. 6(a), 6(d). For comparison, the heat capacity of $MAPbI_3$, and $FAPbI_3$ were also measured and presented in Figs. 6(b), 6(c). The tunneling model (TM) applied to any glassy states, whether structural or physical. There should exist localized excitations of TLS, primarily originating from small atom groups with nearby equilibrium configurations of similar energy [50,51], which

can transit between equilibrium configurations through quantum tunneling even at very low temperatures. The statistical nature of this configurational disorder leads to a random distribution of TLS energies, resulting in a linear temperature dependence of the specific heat [10]. As shown in Figs. 6(a), 6(c), both MA_4InCl_7 and disordered $FAPbI_3$ exhibit upturns at low temperatures, which are attributed to the contribution of the TLS linear term. However, $MAPbI_3$ tends to follow the Debye model at ultralow temperatures and does not display TLS. Furthermore, we have conducted a quadratic polynomial fit to the measured specific heat data curves C_p/T vs T^2 for MA_4InCl_7 , $MAPbI_3$, and $FAPbI_3$. As shown in Fig. 6(d), the presence of a linear term of MA_4InCl_7 at low temperatures is observed, with a TLS linear coefficient approximately $0.86 \text{ mJ mol}^{-1} \text{ K}^{-2}$. In contrast, the linear term of $MAPbI_3$ is essentially zero, indicating that it may exhibit crystalline behavior.